Mesons with beauty and charm: New horizons in spectroscopy

Estia J. Eichten[*] and Chris Quigg[†]

Fermi National Accelerator Laboratory, P.O. Box 500, Batavia, Illinois 60510, USA

The B_c^+ family of $(c\bar{b})$ mesons with beauty and charm is of special interest among heavy quarkonium systems. The B_c^+ mesons are intermediate between $(c\bar{c})$ and $(b\bar{b})$ states both in mass and size, so many features of the $(c\bar{b})$ spectrum can be inferred from what we know of the charmonium and bottomonium systems. The unequal quark masses mean that the dynamics may be richer than a simple interpolation would imply, in part because the charmed quark moves faster in B_c than in the J/ψ. Close examination of the B_c^+ spectrum can test our understanding of the interactions between heavy quarks and antiquarks and may reveal where approximations break down. Whereas the J/ψ and Υ levels that lie below the flavor threshold are metastable with respect to strong decays, the B_c ground state is absolutely stable against strong or electromagnetic decays. Its dominant weak decays arise from $\bar{b} \to \bar{c}W^{\star+}$, $c \to sW^{\star+}$, and $c\bar{b} \to W^{\star+}$ transitions, where $W^\star$ designates a virtual weak boson. Prominent examples of the first category are quarkonium transmutations such as $B_c^+ \to J/\psi\pi^+$ and $B_c^+ \to J/\psi\ell^+\nu_\ell$, where J/ψ designates the $(c\bar{c})$ $1S$ level. The high data rates and extraordinarily capable detectors at the Large Hadron Collider give renewed impetus to the study of mesons with beauty and charm. Motivated by the recent experimental searches for the radially excited B_c states, we update the expectations for the low-lying spectrum of the B_c system. We make use of lattice QCD results, a novel treatment of spin splittings, and an improved quarkonium potential to obtain detailed predictions for masses and decays. We suggest promising modes in which to observe excited states at the LHC. The $3P$ and $3S$ states, which lie close to or just above the threshold for strong decays, may provide new insights into the mixing between quarkonium bound states and nearby two-body open-flavor channels. Searches in the $B^{(*)}D^{(*)}$ final states could well reveal narrow resonances in the $J^P = 0^-$, 1^-, and 2^+ channels and possibly in the $J^P = 0^+$ and 1^+ channels at threshold. Looking further ahead, the prospect of very-high-luminosity e^+e^- colliders capable of producing tera-Z samples raises the possibility of investigating B_c spectroscopy and rare decays in a controlled environment.

I. INTRODUCTION

Although the lowest-lying $(c\bar{b})$ meson has long been established, the spectrum of excited states is little explored. The ATLAS experiment at CERN's Large Hadron Collider reported the observation of a radially excited B_c state [1], but this sighting was not confirmed by the LHCb experiment [2]. The unsettled experimental situation and the large datasets now available for analysis make it timely for us to provide up-to-date theoretical expectations for the spectrum and decay patterns of narrow $(c\bar{b})$ states and for their production in hadron colliders [3]. New work from the CMS Collaboration [4]

[*]eichten@fnal.gov
[†]quigg@fnal.gov

shows the way toward exploiting the potential of $(c\bar{b})$ spectroscopy.

A. What we know of the B_c mesons

The possibility of a spectrum of narrow B_c states was first suggested by Eichten and Feinberg [5]. Anticipating the copious production of b-quarks at Fermilab's Tevatron Collider and CERN's Large Electron-Positron Collider (LEP), we presented a comprehensive portrait of the spectroscopy of the B_c meson and its long-lived excited states [6], based on then-current knowledge of the interaction between heavy quarks derived from $(c\bar{c})$ and $(b\bar{b})$ bound states, within the framework of nonrelativistic quantum mechanics [7]. Surveying four representative potentials, we characterized the mass of the $J^P = 0^-$ ground state as $M(B_c) \approx 6258 \pm 20$ MeV. A small number of B_c candidates appeared in hadronic Z^0 decays at LEP. The CDF Collaboration observed the decay $B_c^\pm \to J/\psi\ell^\pm\nu$ in 1.8-TeV $\bar{p}p$ collisions at the Fermilab Tevatron [8], estimating the mass as $M(B_c) \approx 6400 \pm 411$ MeV. (The generic

lepton ℓ represents an electron or muon.) Subsequent work by the CDF [9], D0 [10], and LHCb [11] Collaborations has refined the mass to $M(B_c) = 6274.9 \pm 0.8$ MeV [12], with the most precise determinations coming from fully reconstructed final states such as $J/\psi\pi^+$.

Investigations based on the spacetime lattice formulation of QCD aim to provide *ab initio* calculations that incorporate the full dynamical content of the theory of strong interactions. Before the nonleptonic B_c decays had been observed, a first unquenched lattice QCD prediction, incorporating $2 + 1$ dynamical quark flavors $(u/d, s)$ found $M(B_c) = 6304 \pm 12^{+18}_{-0}$ MeV [13], where the first error bar represents statistical and systematic uncertainties and the second characterizes heavy-quark discretization effects. Calculations incorporating $2 + 1 + 1$ dynamical quark flavors $(u/d, s, c)$ [14] yield $M(1^1S_0) = 6278 \pm 9$ MeV, in impressive agreement with the measured B_c mass, and predict $M(2^1S_0) = 6894 \pm 19 \pm 8$ MeV [15].

Three distinct elementary processes contribute to the decay of B_c: the individual decays $\bar{b} \to \bar{c}W^{\star+}$ and $c \to sW^{\star+}$ of the two heavy constituents, and the annihilation $c\bar{b} \to W^{\star+}$ through a virtual W-boson. Several examples of the $\bar{b} \to \bar{c}$ transition have been observed, including the final states $J/\psi\ell^+\nu_\ell$, $J/\psi\pi^+$, $J/\psi K^+$, $J/\psi\pi^+\pi^+\pi^-$, $J/\psi\pi^+K^+K^-$, $J/\psi\pi^+\pi^+\pi^+\pi^-\pi^-$, $J/\psi D_s^+$, $J/\psi D_s^{\star+}$, and $J/\psi\pi^+\bar{p}p$; and $\psi(2S)\pi^+$. A single channel, $B_s^0\pi^+$, representing the $c \to s$ transition is known. The annihilation mechanism, which would lead to final states such as $\tau^+\nu_\tau$ and $\bar{p}p\pi^+$, has not yet been established. The observed lifetime, $\tau(B_c) = (0.507 \pm 0.009)$ ps [12], is consistent with theoretical expectations [16,17]. Predictions for partial decay rates (or relative branching fractions) await experimental tests. Some recent theoretical works explore the potential of rare B_c decays [18].

Until recently, the only evidence reported for a $(c\bar{b})$ excited state was presented by the ATLAS Collaboration [1] in pp collisions at 7 and 8 TeV, in samples of 4.9 and 19.2 fb^{-1}. They observed a new state at 6842 ± 7 MeV in the $M(B_c^\pm\pi^+\pi^-) - M(B_c^\pm) - 2M(\pi^\pm)$ mass difference, with $B_c^\pm$ detected in the $J/\psi\pi^\pm$ mode. The mass $(527 \pm 7$ MeV above $\langle M(1S)\rangle)$ and decay of this state are broadly in line with expectations for the second s-wave state, $B_c^\pm(2S)$. In addition to the nonrelativistic potential-model calculations cited above, the HPQCD Collaboration has presented preliminary results from a lattice calculation using $2 + 1 + 1$ dynamical fermion flavors and highly improved staggered quark correlators [19]. They report $M(2^1S_0) = 6892 \pm 41$ MeV, which is 576.5 ± 41 MeV above $\langle M(1S)\rangle$). This result and the NRQCD prediction [14] lie above the ATLAS report by 1 and 2 standard deviations, respectively. The significance of the discrepancy is limited for the moment by lattice uncertainties. A plausible interpretation has been that ATLAS might have observed the transition $B_c^*(2S) \to B_c^*(1S)\pi^+\pi^-$, missing

the low-energy photon from the subsequent $B_c^* \to B_c\gamma$ decay, and that the signal is an unresolved combination of 2^3S_1 and 2^1S_0 peaks. A search by the LHCb collaboration in 2 fb^{-1} of 8-TeV pp data yielded no evidence for either $B_c(2S)$ state [2]. As we prepared this article for publication, the CMS Collaboration provided striking evidence for both $B_c(2S)$ levels, in the form of well-separated peaks in the $B_c\pi^+\pi^-$ invariant mass distribution, closely matching the theoretical template [4]. We incorporate these new observations into the discussion that follows in Sec. V A.

B. Analyzing the $(c\bar{b})$ bound states

The nonrelativistic potential picture, motivated by the asymptotic freedom of QCD [20], gave early insight into the nature of charmonium and generated a template for the spectrum of excited states [21]. For more than four decades, it has served as a reliable guide to quarkonium spectroscopy, including the states lying near or just above flavor threshold for fission into two heavy-light mesons that are significantly influenced by coupled-channel effects [22,23].

We view the nonrelativistic potential-model treatment as a stepping stone, not a final answer, however impressive its record of utility. Potential theory does not capture the full dynamics of the strong interaction, and while the standard coupled-channel treatment is built on a plausible physical picture, it is not derived from first principles. Moreover, relativistic effects may be more important for $(c\bar{b})$ than for $(c\bar{c})$. The c-quark moves faster in the B_c meson than in the J/ψ, because it must balance the momentum of a more massive b-quark. One developing area of theoretical research has been to explore methods more robust than nonrelativistic quantum mechanics [17,24,25].

Nonperturbative calculations on a spacetime lattice in principle embody the full content of QCD. This approach is yielding increasingly precise predictions for the masses of $(c\bar{b})$ levels up through the $B_c^{*\prime}(2^3S_1)$ state. It is not yet possible to extract reliable signals for higher-lying states from the lattice, so we rely on potential-model methods to construct a template for the B_c spectrum through the 4^3S_1 level. If experiments should uncover systematic deviations from the expectations we present, they may be taken as evidence of dynamical features absent from the nonrelativistic potential-model paradigm, including—of course—coupling to states above flavor threshold, which we neglect in our calculations of the spectrum.

In the following Sec. II, we develop the theoretical tools required to compute the $(c\bar{b})$ spectrum. In earlier work [6], we examined the Cornell Coulomb-plus-linear potential [22], a power-law potential [26], Richardson's QCD-inspired potential [27], and a second QCD-inspired potential due to Buchmüller and Tye [28], which we took as our reference model. We used a perturbation-theory treatment of spin splittings. Using insights from lattice QCD and

higher-order perturbative calculations, we construct a new potential that differs in detail from those explored in earlier work. We also use lattice results and rich experimental information on the $(c\bar{c})$ and $(b\bar{b})$ spectra to refine the treatment of spin splittings. We present our expectations for the spectrum of narrow states in Sec. III. We consider decays of the narrow states in Sec. IV, updating the results we gave in Ref. [6]. We compute differential and integrated cross sections for the narrow B_c levels in proton-proton collisions at the Large Hadron Collider in Sec. V. Putting all these elements together, we show how to unravel the $2S$ levels and explore how higher levels might be observed. Prospects for a future $e^+ e^- \to$ tera-Z machine appear in Sec. VI. We draw some conclusions and look ahead in Sec. VII.

II. THEORETICAL PRELIMINARIES

We take as our starting point a Coulomb-plus-linear potential (the "Cornell potential" [22]),

$$V(r) = -\frac{\kappa}{r} + \frac{r}{a^2}, \tag{1}$$

where $\kappa \equiv 4\alpha_s/3 = 0.52$ and $a = 2.34$ GeV^{-1} were chosen to fit the quarkonium spectra. Analysis of the J/ψ and Υ families led to the choices

$$m_c = 1.84 \text{ GeV} \quad m_b = 5.18 \text{ GeV}. \tag{2}$$

This simple form has been modified to incorporate running of the strong coupling constant in Refs. [27,28], among others, using the perturbative-QCD evolution equation at leading order and beyond. At distances relevant for confinement, perturbation theory ceases to be a reliable guide. It is now widely held, following Gribov [29], that as a result of quantum screening α_s approaches a critical, or frozen, value at long distances (low-energy scales). In a light $(q\bar{q})$ system, Gribov estimated

$$\alpha_s \to \bar{\alpha}_s = \frac{3\pi}{4}(1 - \sqrt{2/3}) \approx 0.14\pi = 0.44. \tag{3}$$

We incorporate the spirit of this insight into a new version of the Coulomb-plus-linear form that we call the "frozen-α_s potential."

The long-range part is the standard Cornell linear term. To obtain the Coulomb piece, we convert the four-loop running of $\alpha_s(q)$ in momentum space [30] to the behavior in position space using the method of [31], with an important modification. We set $\alpha_s(q = 1.6 \text{ GeV}) = 0.338$ and evolve with three active quark flavors. To enforce saturation of $\alpha_s(r)$ at long distances, we alter the recipe of Ref. [31], replacing the identification $q = 1/r \exp(\gamma_E)$, where $\gamma_E = 0.57721\ldots$ is Euler's constant, with the damped form $q = 1/[(r \exp(\gamma_E)^2 + \mu^2]^{1/2}$. For our reference potential, we have chosen the damping parameter $\mu = 1.2$ GeV.
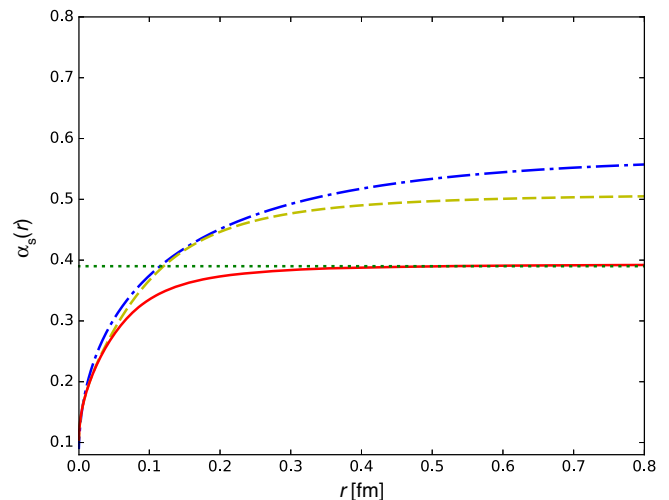

FIG. 1. Dependence of the running coupling $\alpha_s(r)$ on the interquark separation r. The strong coupling for our chosen potential is shown in the solid red curve. Those corresponding to the Cornell potential (green dots) [22], Richardson potential (blue dash-dotted) [27], and an alternative version of the new potential with $\mu = 0.8$ GeV (gold dashes) are shown for comparison.

The consequent evolution of $\alpha_s(r)$ is plotted as the solid red curve in Fig. 1, where we also show an alternative choice of $\mu = 0.8$ GeV (dashed gold curve), the constant α_s of the original Cornell potential (dotted green curve), and $\alpha_s(r)$ corresponding to the Richardson potential (dot-dashed blue curve).

We plot in Fig. 2 the frozen-α_s potential for both our chosen example, $\mu = 1.2$ GeV, and the alternative, $\mu = 0.8$ GeV. There we also show the Richardson and
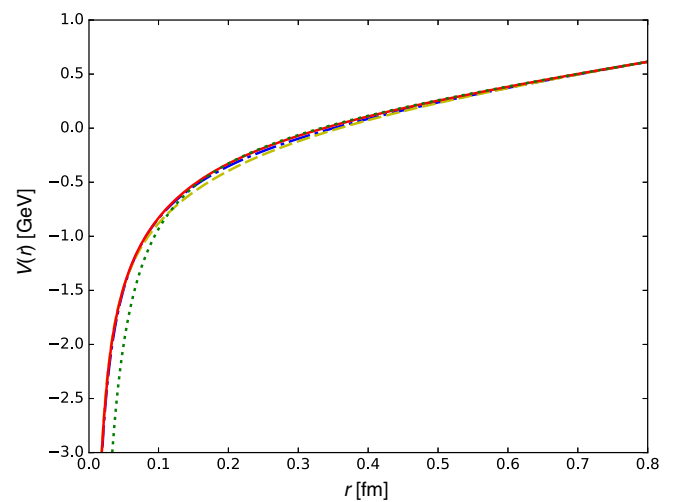

FIG. 2. Dependence of quarkonium potentials $V(r)$ on the interquark separation r. Our frozen-α_s potential is shown in the solid red curve. The Cornell potential (green dots) [22], Richardson potential (blue dash-dotted) [27], and an alternative version of the new potential with $\mu = 0.8$ GeV (gold dashes) are shown for comparison.

TABLE I. *P*-state masses [12] and splittings, in MeV.

State	$2P(c\bar{c})$	$2P(b\bar{b})$	$3P(b\bar{b})$
$\chi_0(^3P_0)$	3414.71 ± 0.30	9859.44 ± 0.52	10232.5 ± 0.64
$\chi_1(^3P_1)$	3510.67 ± 0.05	9892.78 ± 0.4	10255.46 ± 0.55
$h(^1P_1)$	3525.38 ± 0.11	9899.3 ± 0.8	10259.8 ± 1.12
$\chi_2(^3P_2)$	3556.17 ± 0.07	9912.21 ± 0.4	10268.85 ± 0.55
^3P_J centroid, $\langle\chi\rangle$	3525.29 ± 0.01	9899.87 ± 0.17	10260.35 ± 0.31
$h - \langle\chi\rangle$	0.09 ± 0.11	-0.57 ± 0.82	-0.55 ± 1.25
$\chi_1(^3P_1) - \chi_0(^3P_0)$	95.96 ± 0.30	33.34 ± 0.66	22.96 ± 0.84
$\chi_2(^3P_2) - \chi_0(^3P_2)$	45.5 ± 0.09	19.43 ± 0.57	13.39 ± 0.78

Cornell potentials. All coincide at large distances. The Cornell potential is deeper at short distances than any of the potentials that take account of the evolution of α_s. For the convenience of others who may wish to apply the new potential, we present values of $\alpha_s(r)$ suitable for interpolation in the Appendix.

We presented the general formalism for spin-dependent interactions as laid out by Eichten and Feinberg [5] and Gromes [32] in Sec. II B of Ref. [6], where we took a perturbative approach to the spin-orbit and tensor interactions. In the intervening time, the charmonium and bottomonium spectra have been mapped in detail, as summarized in Table I. This wealth of information leads us now to choose a more phenomenological approach.

We write the spin-dependent contributions to the $(c\bar{b})$ masses as

$$\Delta = \sum_{k=1}^{4} T_k, \tag{4}$$

where the individual terms are

$$T_1 = \frac{\langle\vec{L}\cdot\vec{s}_i\rangle}{2m_i^2}\tilde{T}_1(m_i, m_j) + \frac{\langle\vec{L}\cdot\vec{s}_j\rangle}{2m_j^2}\tilde{T}_1(m_j, m_i)$$

$$T_2 = \frac{\langle\vec{L}\cdot\vec{s}_i\rangle}{m_i m_j}\tilde{T}_2(m_i, m_j) + \frac{\langle\vec{L}\cdot\vec{s}_j\rangle}{m_i m_j}\tilde{T}_2(m_j, m_i)$$

$$T_3 = \frac{\langle\vec{s}_i\cdot\vec{s}_j\rangle}{m_i m_j}\tilde{T}_3(m_i, m_j)$$

$$T_4 = \frac{\langle S_{ij}\rangle}{m_i m_j}\tilde{T}_4(m_i, m_j), \tag{5}$$

$\vec{s}_i$ and $\vec{s}_j$ are the heavy-quark spins, $\vec{S} = \vec{s}_i + \vec{s}_j$ is the total spin, $\vec{L}$ is the orbital angular momentum of quark and antiquark in the bound state, $S_{ij} = 4[3(\vec{s}_i\cdot\hat{n})(\vec{s}_j\cdot\hat{n}) - \vec{s}_i\cdot\vec{s}_j]$ is the tensor operator, and $\hat{n}$ is an arbitrary unit vector.

We will deal with the hyperfine interaction T_3 momentarily. We express the other $\tilde{T}_k$ as

$$\tilde{T}_1(m_i, m_j) = -\left\langle\frac{1}{r}\frac{dV}{dR}\right\rangle + 2\tilde{T}_2(m_i, m_j)$$

$$\tilde{T}_2(m_i, m_j) = \frac{4\tilde{c}_2}{3}\left\langle\frac{\alpha_s(r)}{r^3}\right\rangle$$

$$\tilde{T}_4(m_i, m_j) = \frac{\tilde{c}_4}{3}\left\langle\frac{\alpha_s(r)}{r^3}\right\rangle, \tag{6}$$

where we have introduced the phenomenological coefficients $\tilde{c}_2$ and $\tilde{c}_4$, which take the value unity in the perturbative approach.

We extract values of $\tilde{T}_2$ and $\tilde{T}_4$ for the observed levels that appear in Table I. These are shown as the boldface entries in Table II. Then, we combine the definitions in Eq. (6) with our calculated values of $\langle\alpha_s/r^3\rangle$ to determine $\tilde{c}_2$ and $\tilde{c}_4$ in the $(c\bar{c})$ and $(b\bar{b})$ families. The geometric mean of these values is our estimate for the coefficients in the $c\bar{b}$ system. We insert these back into Eq. (6) to estimate the values of $\tilde{T}_2$ and $\tilde{T}_4$ for the B_c family. For completeness, we include our evaluations of $\langle(1/r)dV/dr\rangle$ in the table.

For the J/ψ and Υ families, composed of equal-mass heavy quarks, the familiar LS coupling scheme, in which states are labeled by $n^{2S+1}L_J$, is apt. When the quark masses are unequal, as in the case at hand, spin-dependent terms in the Hamiltonian mix the spin-singlet and spin-triplet $J = L$ states. We define

TABLE II. Values of $\tilde{T}_2$ and $\tilde{T}_4$ extracted from data (bold) and the inferred values of the phenomenological coefficients $\tilde{c}_2$ and $\tilde{c}_4$ for the J/ψ and Υ families, from which the coefficients for the $(c\bar{b})$ system are derived.

System	$\tilde{T}_2$	$\tilde{T}_4$	$\left\langle\frac{\alpha_s(r)}{r^3}\right\rangle$ (GeV³)	$\tilde{c}_2$	$\tilde{c}_4$	$\left\langle\frac{1}{r}\frac{dV}{dr}\right\rangle$ (GeV³)
$1P(c\bar{c})$	**0.088**	**0.0308**	0.0527	1.25	1.77	0.141
$1P(b\bar{b})$	**0.258**	**0.0835**	0.220	0.82	0.99	0.383
$2P(b\bar{b})$	**0.181**	**0.0547**	0.166	0.82	0.99	0.278
$1P(c\bar{b})$	0.119	0.0388	0.0885	1.012	1.316	0.198

$$|nL_L\rangle' = \cos\theta|n^1L_L\rangle + \sin\theta|n^3L_L\rangle,$$
$$|nL_L\rangle = -\sin\theta|n^1L_L\rangle + \cos\theta|n^3L_L\rangle, \qquad (7)$$

where

$$\tan\theta = \frac{2A}{B + \sqrt{B^2 + 4A^2}}, \qquad (8)$$

with

$$A = \frac{1}{4}\sqrt{L(L+1)}\left(\frac{1}{m_c^2} - \frac{1}{m_b^2}\right)\tilde{T}_1 \qquad (9)$$

and

$$B = \frac{1}{4}\left(\frac{1}{m_c^2} + \frac{1}{m_b^2}\right)\tilde{T}_1 + \frac{1}{m_c m_b}\tilde{T}_2 - 2\frac{1}{m_c m_b}\tilde{T}_4. \qquad (10)$$

Then our calculations of the $\tilde{T}_k$ defined in Eq. (6) lead to these values for the mixing angle: $\theta_{2P} = 18.7°$, $\theta_{3D} = -49.2°$, $\theta_{3P} = 21.2°$, $\theta_{4F} = -49.5°$, $\theta_{4D} = -40.3°$. A lattice calculation in quenched QCD [33] gave $\theta_{2P} = 33 \pm 2°$.

The masses of the mixed states are

$$M(nL'_L) = \langle M(nL)\rangle - \frac{1}{2}(B - \sqrt{4A^2 + B^2}),$$

$$M(nL_L) = \langle M(nL)\rangle - \frac{1}{2}(B + \sqrt{4A^2 + B^2}), \qquad (11)$$

where $\langle M(nL)\rangle$ is the nL centroid.

At lowest order, the hyperfine splitting (HFS) between s-wave states, arising from T_3, is given by

$$\Delta_{\text{HFS}}^{(n)} = M(n^3S_1) - M(n^1S_0) = \frac{8\alpha_s|R_{n0}(0)|^2}{9m_c m_b}, \qquad (12)$$

which is susceptible to significant quantum corrections. Rather than make *a priori* calculations of the hyperfine splitting, we adopt the lattice QCD result for the ground state and scale the splittings of excited states according to

$$\frac{\Delta_{\text{HFS}}^{(n)}}{\Delta_{\text{HFS}}^{(1)}} = \frac{|R_{n0}(0)|^2}{|R_{10}(0)|^2}. \qquad (13)$$

III. THE B_c SPECTRUM

The vector meson B_c^*, the 1^3S_1 hyperfine partner of B_c and analog of J/ψ and Υ, has not yet been observed. Modern lattice calculations [14,34,35] give consistent values for the hyperfine splitting $M(B_c^*) - M(B_c) = (53 \pm 7, 54 \pm 7, 55 \pm 3 \text{ MeV})$, so we take the mass of the vector state to be $M(B_c^*) = 6329$ MeV and fix the centroid $\langle M(1S)\rangle$ of the ground-state s-wave doublet at 6315.5 MeV for the lattice.

TABLE III. Calculated excitation energies (in MeV) for $(c\bar{b})$ levels with respect to the $B_c(1S)$ centroid according to potential models and lattice QCD simulations. The potential models have been aligned with the $1S$ doublet centroid at 6315.5 MeV. Communication with states above flavor threshold is neglected.

Level	EQ94 [6]	Lattice QCD	This work
1^1S_0	−54.8	−40.5 [14,34,35]	−40.5
1^3S_1	18.2	13.5 [14,34,35]	13.5
2^3P_0	381	393(17)(7) [35]	377
$2P_1$	411	417(18)(7) [35]	415
$2P_1'$	417	446(30) [33]	423
2^3P_2	428	464(30) [33]	435
2^1S_0	537	561(18)(1) [14]	551
2^3S_1	580	601(19)(1) [14]	582
3^3D_1	693	⋯	691
$3D_2$	693	⋯	690
$3D_2'$	686	⋯	700
3^3D_3	690	⋯	695
3^3P_0	789	⋯	789
$3P_1$	823	⋯	820
$3P_1'$	816	⋯	828
3^3P_2	834	⋯	839
3^1S_0	925	⋯	938
3^3S_1	961	⋯	964
4^3F_2	⋯	⋯	918
$4F_3$	⋯	⋯	906
$4F_3'$	⋯	⋯	922
4^3F_4	⋯	⋯	908
4^3D_1	⋯	⋯	1031
$4D_2$	⋯	⋯	1033
$4D_2'$	⋯	⋯	1040
4^3D_3	⋯	⋯	1038
4^3P_0	⋯	⋯	1121
$4P_1$	⋯	⋯	1149
$4P_1'$	⋯	⋯	1158
4^3P_2	⋯	⋯	1167
4^1S_0	1243	⋯	1257
4^3S_1	1276	⋯	1280

We summarize in Table III predictions for the spectrum of mesons with beauty and charm from our 1994 article [6], lattice QCD calculations, and the present work, expressed as excitations with respect to the $1S$ centroid. Other potential-model calculations, some incorporating relativistic effects, may be found in the works cited in Ref. [7].

Our expectations for the spectrum of states are shown in the Grotrian diagram, Fig. 3, along with several of the lowest-lying open-flavor thresholds. The thresholds for strong decays of excited $(c\bar{b})$ levels are known experimentally to high accuracy, as shown in Table IV. Comparing with the model calculations summarized in Table III, we conclude that two sets of narrow s-wave $(c\bar{b})$ levels will lie below the beauty + charm flavor threshold, in agreement with general arguments [36]. All of the potential models cited in Ref. [7] predict 3^3S_1 masses well above the
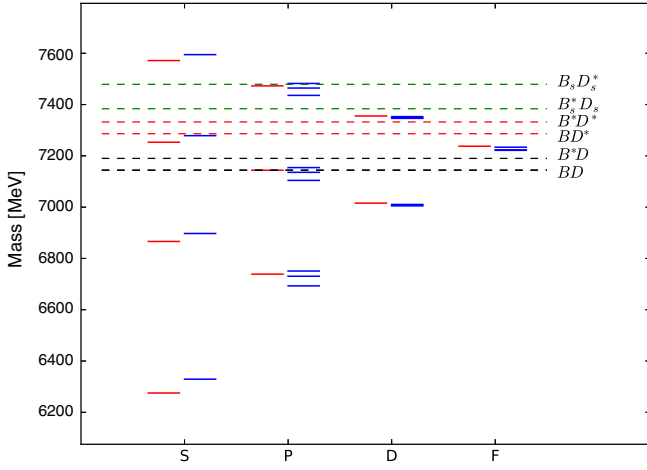
FIG. 3.   Calculated $c\bar{b}$ spectrum, with (spin-singlet, spin-triplet) states shown on the left (right) in red (blue) for each orbital-angular-momentum family S, P, D, F. Dashed lines indicate thresholds for decay into two-body open-flavor channels given in Table IV.

829-MeV BD threshold. For the 3^1S_0 level, only the Ebert et al. prediction does not lie significantly above the B^*D threshold. Lattice QCD calculations do not yet exist for states beyond the $2S$ levels.

IV. DECAYS OF NARROW $(c\bar{b})$ LEVELS

A. Electromagnetic transitions

The only significant decay mode for the 1^3S_1 (B_c^*) state is the magnetic dipole (spin-flip) transition to the ground state, B_c. The M1 rate for transitions between s-wave levels is given by

$$\Gamma_{\mathrm{M1}}(i \rightarrow f + \gamma) = \frac{16\alpha}{3}\mu^2 k^3 (2J_f + 1)|\langle f|j_0(kr/2)|i\rangle|^2, \tag{14}$$

TABLE IV.   Open-flavor $(c\bar{b})$ thresholds and excitations above $1S$ centroid, 6315.5 MeV, for B_c levels, in MeV.

State	Flavor threshold	Excitation energy
B^+D^0	7144.15 ± 0.15	829
B^0D^+	7149.28 ± 0.16	834
$B^{*+}D^0$	7189.48 ± 0.26	874
$B^{*0}D^+$	7194.30 ± 0.26	879
B^+D^{*0}	7286.17 ± 0.15	971
B^0D^{*+}	7289.89 ± 0.16	974
$B^{*+}D^{*0}$	7331.50 ± 0.26	1016
$B^{*0}D^{*+}$	7334.91 ± 0.26	1019
$B_s^0D_s^+$	7335.23 ± 0.20	1020
$B_s^0D_s^{*+}$	7479.09 ± 0.44	1164
$B_s^{*0}D_s^+$	$7383.74^{+1.80}_{-1.50}$	1068
$B_s^{*0}D_s^{*+}$	$7527.60^{+1.84}_{-1.55}$	1212

where the magnetic dipole moment is

$$\mu = \frac{m_b e_c - m_c e_{\bar{b}}}{4m_c m_b} \tag{15}$$

and k is the photon energy.

Apart from that M1 transition, only the electric dipole transitions are important for mapping the $(c\bar{b})$ spectrum. The strength of the electric-dipole transitions is governed by the size of the radiator and the charges of the constituent quarks. The E1 transition rate is given by

$$\Gamma_{\mathrm{E1}}(i \rightarrow f + \gamma) = \frac{4\alpha\langle e_Q\rangle^2}{27} k^3 (2J_f + 1)|\langle f|r|i\rangle|^2 \mathcal{S}_{if}, \tag{16}$$

where the mean charge is

$$\langle e_Q\rangle = \frac{m_b e_c - m_c e_{\bar{b}}}{m_b + m_c}, \tag{17}$$

k is the photon energy, and the statistical factor $\mathcal{S}_{if} = \mathcal{S}_{fi}$ is as defined by Eichten and Gottfried [37]. $\mathcal{S}_{if} = 1$ for $^3S_1 \rightarrow {}^3P_J$ transitions and $\mathcal{S}_{if} = 3$ for allowed E1 transitions between spin-singlet states. The statistical factors for d-wave to p-wave transitions are reproduced in Table V.

The significant M1 and E1 electromagnetic transition rates and the $\pi\pi$ cascade rates are given in Table VI, along with the total widths in the absence of fission decays.

B. Hadronic transitions

We evaluate the rates for hadronic transitions between $(c\bar{b})$ levels according to the prescription we detailed in Sec. III B of Ref. [6]. The results are included in Table VI. Dipion cascades to the ground-state doublet are the dominant decay modes of 2^3S_1 and 2^1S_0 and will be key to characterizing those states, as we shall discuss in Sec. V A.

As observed long ago by Brown and Cahn [38], an amplitude zero imposed by chiral symmetry pushes the $\pi^+\pi^-$ invariant mass distribution to higher invariant masses than phase space alone would predict. In its simplest form, this analysis yields a universal form for the normalized dipion invariant mass distribution in quarkonium cascades $\Phi' \rightarrow \Phi\pi^+\pi^-$,

TABLE V.   Statistical factor $\mathcal{S}_{if} = \mathcal{S}_{fi}$ for $^3P_J \rightarrow {}^3D_{J'} + \gamma$ and $^3D_J \rightarrow {}^3P_{J'} + \gamma$ transitions.

J	J'	$\mathcal{S}_{if}$
0	1	2
1	1	1/2
1	2	9/10
2	1	1/50
2	2	9/50
2	3	18/25

TABLE VI. Total widths Γ and branching fractions $\mathcal{B}$ for principal decay modes of $(c\bar{b})$ states below threshold, updating Table IX of Ref. [6]. Dissociation into BD, etc., will dominate over the tabulated decay modes for states above threshold.

Decay mode	k_γ (keV)	Branching fraction (%)
1^1S_0 (6275): Weak decays		
1^3S_1 (6329): $\Gamma = 0.144$ keV		
$1^1S_0 + \gamma$	54	100
2^3P_0 (6692): $\Gamma = 53.1$ keV		
1^3S_1 (6329)	354	100
$2P_1$ (6730): $\Gamma = 72.5$ keV		
1^3S_1 (6329)	389	86.2
1^1S_0 (6275)	440	13.7
$2P_1'$ (6738): $\Gamma = 99.9$ keV		
1^1S_0 (6275)	448	92.4
1^3S_1 (6329)	397	7.51
2^3P_2 (6750): $\Gamma = 79.7$ keV		
1^3S_1 (6329)	409	100
2^1S_0 (6866): $\Gamma = 73.1$ keV		
$1^1S_0 + \pi\pi$		81.1
$2P_1'$ (6738)	126	16.5
$2P_1$ (6730)	134	2.24
2^3S_1 (6897): $\Gamma = 76.8$ keV		
$1^3S_1 + \pi\pi$		65.0
2^3P_0 (6692)	201	7.66
$2P_1$ (6730)	165	11.5
$2P_1'$ (6738)	157	1.13
2^3P_2 (6750)	145	14.6
$3D_2$ (7005): $\Gamma = 93.7$ keV		
$1^1S_0 + \pi\pi$		12.2
$1^3S_1 + \pi\pi$		9.0
$2P_1$ (6730)	270	29.1
$2P_1'$ (6738)	262	42.3
2^3P_2 (6750)	250	7.24
3^3D_1 (7006): $\Gamma = 117$ keV		
$1^3S_1 + \pi\pi$		17.0
2^3P_0 (6692)	306	53.4
$2P_1$ (6730)	270	25.3
$2P_1'$ (6738)	262	2.62
2^3P_2 (6750)	251	1.51
3^3D_3 (7010): $\Gamma = 87.2$ keV		
$1^3S_1 + \pi\pi$		22.9
2^3P_2 (6750)	255	77.0
$3D_2'$ (7015): $\Gamma = 92.1$ keV		
$1^1S_0 + \pi\pi$		9.2

(Table continued)

TABLE VI. *(Continued)*

Decay mode	k_γ (keV)	Branching fraction (%)
$1^3S_1 + \pi\pi$		12.4
$2P_1'$ (6738)	272	37.2
$2P_1$ (6730)	279	41.0
3^3P_0 (7104): $\Gamma = 60.9$ keV		
1^3S_1 (6329)	733	46.4
2^3S_1 (6897)	204	45.0
3^3D_1 (7006)	97	8.44
$3P_1$ (7135): $\Gamma = 87.1$ keV		
1^3S_1 (6329)	761	32.6
1^1S_0 (6275)	809	6.24
2^3S_1 (6897)	234	40.4
2^1S_0 (6866)	264	8.39
$3D_2$ (7005)	129	4.74
$3D_2'$ (7015)	119	4.55
3^3D_1 (7006)	128	2.88
$3P_1'$ (7143): $\Gamma = 113$ keV		
1^1S_0 (6275)	816	32.9
1^3S_1 (6329)	768	3.88
2^1S_0 (6866)	272	47.0
2^3S_1 (6897)	242	5.15
$3D_2'$ (7015)	127	4.22
$3D_2$ (7005)	137	6.72
3^3P_2 (7154): $\Gamma = 100$ keV		
1^3S_1 (6329)	777	35.2
2^3S_1 (6897)	252	49.2
$3D_2$ (7005)	147	1.09
$3D_2'$ (7015)	137	1.18
3^3D_1 (7006)	146	0.16
3^3D_3 (7010)	142	13.0
$4F_3$ (7221): $\Gamma = 77.6$ keV		
$3D_2$ (7005)	213	52.4
$3D_2'$ (7015)	203	42.8
3^3D_3 (7010)	208	4.71
4^3F_4 (7223): $\Gamma = 79.9$ keV		
3^3D_3 (7010)	210	100
4^3F_2 (7233): $\Gamma = 95.3$ keV		
$3D_2$ (7005)	225	6.73
$3D_2'$ (7015)	215	7.96
3^3D_1 (7006)	224	84.8
3^3D_3 (7010)	220	0.42
$4F_3'$ (7237): $\Gamma = 89.9$ keV		
$3D_2'$ (7015)	218	47.4
$3D_2$ (7005)	228	52.5

$$\frac{1}{\Gamma}\frac{d\Gamma}{d\mathcal{M}} = \text{constant} \times \frac{|\vec{K}|}{M_{\Phi'}^2}(2x^2 - 1)^2\sqrt{x^2 - 1}, \quad (18)$$

where $x = \mathcal{M}/2m_\pi$ and $\vec{K}$ is the three-momentum carried by the pion pair. The soft-pion expression (18) describes the depletion of the dipion spectrum at low invariant masses observed in the transitions $\psi(2S) \to \psi(1S)\pi\pi$, $\Upsilon(2S) \to \Upsilon(1S)\pi\pi$, and $\Upsilon(3S) \to \Upsilon(2S)\pi\pi$, but fails to account for structures in the $\Upsilon(3S) \to \Upsilon(1S)\pi\pi$ spectrum [39]. We expect the $3S$ levels to lie above flavor threshold in the $(c\bar{b})$ system and so to have very small branching fractions for cascade decays (but see the final paragraph of Sec. V A).

C. Properties of $(c\bar{b})$ wave functions at the origin

For quarks bound in a central potential, it is convenient to separate the Schrödinger wave function into radial and angular pieces, as $\Psi_{n\ell m}(\vec{r}) = R_{n\ell}(r)Y_{\ell m}(\theta, \phi)$, where n is the principal quantum number, ℓ and m are the orbital angular momentum and its projection, $R_{n\ell}(r)$ is the radial wave function, and $Y_{\ell m}(\theta, \phi)$ is a spherical harmonic [40]. The Schrödinger wave function is normalized, $\int d^3\vec{r}|\Psi_{n\ell m}(\vec{r})|^2 = 1$, so that $\int_0^\infty r^2 dr|R_{n\ell}(r)| = 1$. The value of the radial wave function, or its first non-vanishing derivative, at the origin,

$$R_{n\ell}^{(\ell)}(0) \equiv \left.\frac{d^\ell R_{n\ell}(r)}{dr^\ell}\right|_{r=0}, \quad (19)$$

is required to evaluate pseudoscalar decay constants and production rates through heavy-quark fragmentation. Our calculated values of $|R_{n\ell}^{(\ell)}(0)|^2$ are given in Table VII.

The pseudoscalar decay constant f_{B_c}, which enters the calculations of annihilation decays such as $c\bar{b} \to W^+ \to \tau^+ + \nu_\tau$, is defined by

$$\langle 0|A_\mu(0)|B_c(q)\rangle = if_{B_c}\mathsf{V}_{cb}q_\mu, \quad (20)$$

where A_μ is the axial-vector part of the charged weak current, V_{cb} is an element of the Cabibbo-Kobayashi-Maskawa quark-mixing matrix, and q_μ is the four-momentum of the B_c. Its counterpart for the vector state is

$$\langle 0|V_\mu(0)|B_c^*(q)\rangle = if_{B_c^*}\mathsf{V}_{cb}\varepsilon_\mu^*, \quad (21)$$

where V_μ is the vector part of the charged weak current and ε_μ^* is the polarization vector of the B_c^*. The ground-state pseudoscalar and vector decay constants are given in terms of the wave function at the origin by the Van Royen-Weisskopf formula [41], generically

$$f_{B_c^{(*)}}^2 = \frac{3|R_{10}(0)|^2}{\pi M}\bar{C}^2(\alpha_s), \quad (22)$$

where the leading-order QCD correction is given by [42]

TABLE VII. Squares of radial wave functions at the origin and related quantities [cf. Eq. (19)] for $(c\bar{b})$ mesons.

Level	$|R_{n\ell}^{(\ell)}(0)|^2$
$1S$	1.994 GeV^3
$2P$	0.3083 GeV^5
$2S$	1.144 GeV^3
$3D$	0.0986 GeV^7
$3P$	0.3939 GeV^5
$3S$	0.9440 GeV^3
$4F$	0.0493 GeV^9
$4D$	0.1989 GeV^7
$4P$	0.4540 GeV^5
$4S$	0.8504 GeV^3

$$\bar{C}^2(\alpha_s) = 1 - \frac{\alpha_s}{\pi}\left(\delta^{P,V} - \frac{m_c - m_b}{m_c + m_b}\ln\frac{m_c}{m_b}\right), \quad (23)$$

and

$$\delta^P = 2; \qquad \delta^V = 8/3. \quad (24)$$

Choosing the representative value $\alpha_s = 0.38$, and using the quark masses given in Eq. (2), we find

$$\bar{C}(\alpha_s) = \begin{array}{l} 0.904, \text{P} \\ 0.858, \text{V} \end{array}. \quad (25)$$

Consequently, we estimate the ground-state meson decay constants as

$$f_{B_c} = 498 \text{ MeV}; \qquad f_{B_c^*} = 471 \text{ MeV}, \quad (26)$$

so that $f_{B_c^*}/f_{B_c} = 0.945$. The compact size of the $(c\bar{b})$ system enhances the pseudoscalar decay constant relative to f_π and f_K.

This is to be compared to a state-of-the-art lattice evaluation [43], $f_{B_c} = 434 \pm 15$ MeV, which entails improved nonrelativistic QCD for the valence b-quark and the highly improved staggered quark action for the lighter quarks on gluon field configurations that include the effect of u/d, s, and c quarks in the sea with the u/d quark masses going down to physical values. The same calculation yields $f_{B_c^*}/f_{B_c} = 0.988 \pm 0.027$. A calculation in the framework of QCD sum rules gives $f_{B_c} = 528 \pm 19$ MeV [44].

V. PRODUCTION OF $(c\bar{b})$ STATES AT THE LARGE HADRON COLLIDER

We present in Table VIII cross sections for the production of B_c states at the Large Hadron Collider, calculated using the framework of the BCVEGPY2.2 generator [45], which we have extended to include the production of $3P$

TABLE VIII.   Production rates (in nanobarn) for $(c\bar{b})$ states in pp collisions at the LHC. The production rates were calculated using the BCVEGPY2.2 generator of Ref. [45], extended to include the production of $3P$ states. Color-octet contributions to s-wave production are small; we show them (following |) only for the $1S$ states.

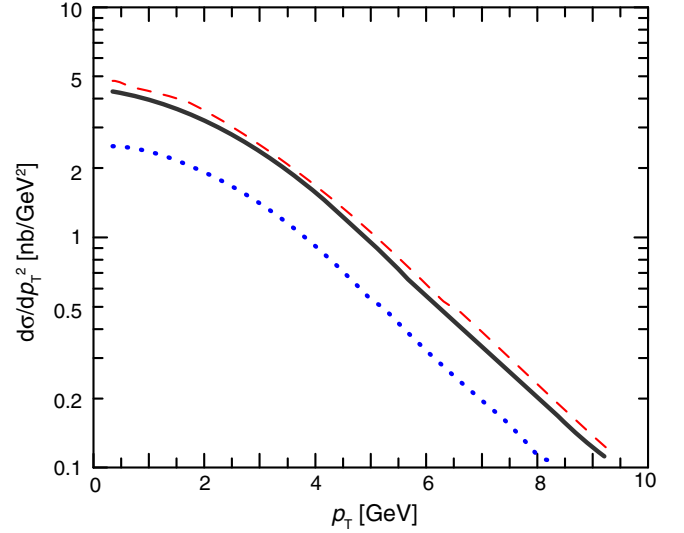| $(c\bar{b})$ level	$\sigma(\sqrt{s}=8\text{ TeV})$	$\sigma(\sqrt{s}=13\text{ TeV})$	$\sigma(\sqrt{s}=14\text{ TeV})$
1^1S_0	46.8|1.01	80.3|1.75	88.0|1.90
1^3S_1	123.0|4.08	219.1|6.97	237.0|7.55
2^3P_0	1.113	1.959	2.108
2^3P_1	2.676	4.783	5.214
2^1P_1	3.185	5.702	6.166
2^3P_2	6.570	11.57	12.64
2^1S_0	9.58	16.94	18.45
2^3S_1	23.46	41.72	45.53
3^3P_0	0.915	1.642	1.806
3^3P_1	2.263	4.082	4.478
3^1P_1	2.695	4.817	5.287
3^3P_2	5.53	9.98	10.90
3^1S_0	4.23	7.53	8.08
3^3S_1	10.16	18.21	19.83

FIG. 5.   Transverse momentum distribution of B_c produced in pp collisions at $\sqrt{s} = 8$ TeV (dotted blue curve), $\sqrt{s} = 13$ TeV (solid black curve), and $\sqrt{s} = 14$ TeV (dashed red curve), calculated using BCVEGPY2.2 [45]. Small shape variations are statistical fluctuations.

states. Cross sections for the physical $(2,3)P_1^{(\prime)}$ states are appropriately weighted mixtures of the $^3P_1$ and $^1P_1$ cross sections.

The rapidity distributions (for B_c^* production, Fig. 4) and transverse-momentum distributions (shown for B_c production, Fig. 5) are similar in character for $\sqrt{s} = 8$, 13, and 14 TeV. The rapidity distributions for low-lying $(c\bar{b})$ states

are shown in Fig. 6. The acceptance of the CMS and ATLAS detectors covers central pseudorapidity $|\eta| \leq 2.5$, whereas the geometrical acceptance of the LHCb detector is characterized by $2 \leq \eta \leq 5$. For comparison, approximately 68% of the B_c^* cross section lies within $|y| \leq 2.5$, and approximately 22% is produced at forward rapidities $y > 2$. Similar fractions hold for all the $(c\bar{b})$ levels.

FIG. 4.   Rapidity distribution for production of B_c^* in pp collisions at $\sqrt{s} = 8$ TeV (dotted blue curve), $\sqrt{s} = 13$ TeV (solid black curve), and $\sqrt{s} = 14$ TeV (dashed red curve), calculated using BCVEGPY2.2 [45]. The bin width is $\Delta y = 0.5$. The mild asymmetries are statistical fluctuations.
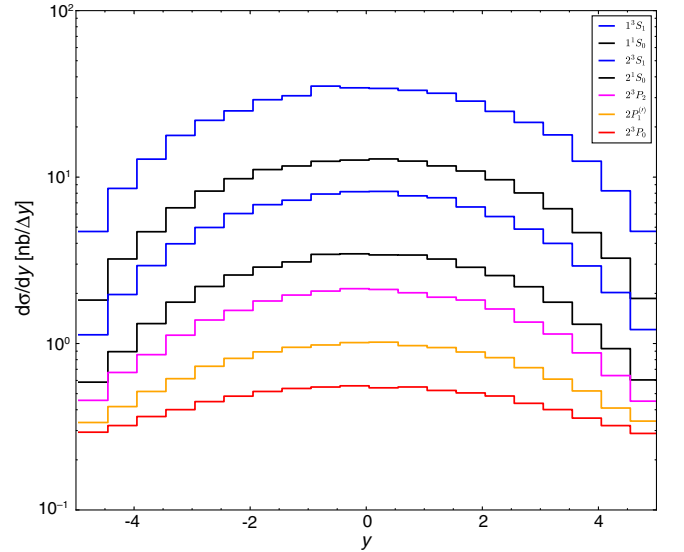

FIG. 6.   Rapidity distributions for the production of low-lying $(c\bar{b})$ states in pp collisions at $\sqrt{s} = 13$ TeV, calculated using BCVEGPY2.2 [45]. From highest to lowest, the histograms refer to production of the 1^3S_1, 1^1S_0, 2^3S_1, 2^1S_0, 2^3P_2, $2P_{1^{(\prime)}}$, 2^3P_0 levels.
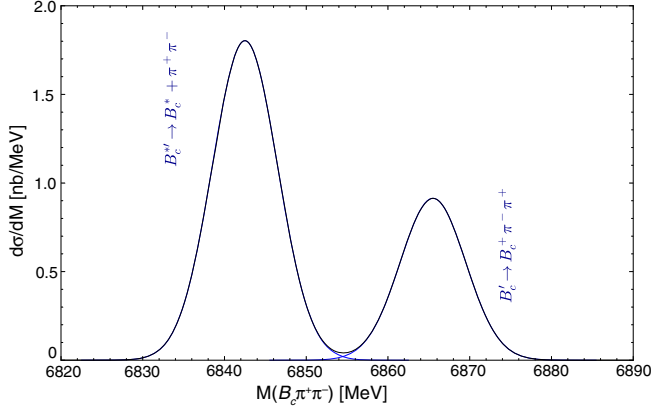
FIG. 7. Calculated positions and relative strengths of the two-pion cascades $B_c(2S) \to B_c(1S)\pi^+\pi^-$, represented as Gaussian line shapes with standard deviation of 4 MeV. Production rates are given in Table VIII and branching fractions in Table VI. We assume that the photon in the transition $B_c^* \to B_c + \gamma$ is not included in the reconstruction. Rates confined to rapidity $|y| \leq 2.5$ are $0.68\times$ those shown.

A. Dipion cascades

The path to establishing excited states will proceed by resolving two separate peaks in the invariant mass distributions associated with the cascades $B_c' \to B_c\pi^+\pi^-$ and $B_c^{*'} \to B_c^* + \pi^+\pi^-$, $B_c^* \to B_c + \gamma$ (gamma unobserved). The splitting between the peaks is set by the difference of mass differences,

$$\Delta_{21} \equiv [M(B_c^{*'}) - M(B_c')] - [M(B_c^*) - M(B_c)], \quad (27)$$

generically expected to be negative [46]. The corresponding quantity is approximately -64 MeV in the $(c\bar{c})$ family and -37 MeV in the $(b\bar{b})$ family [12]. For the $(c\bar{b})$ system, a modern lattice simulation [14] gives $\Delta_{21} = -15$ MeV, whereas the result of our potential-model calculation is -23 MeV. In these circumstances, the undetected four-momentum of the photon means that the reconstructed "B_c^*" mass should correspond to the lower peak.

We show an example of what is to be expected in Fig. 7, taking the direct production cross sections (with no rapidity cuts) from Table VIII and the branching fractions from Table VI. The relative heights of (and relative number of events in) the peaks measures the ratio

$$\mathcal{R} \equiv \frac{\sigma(B_c^{*'} + X)\mathcal{B}(B_c^{*'} \to B_c^* + \pi^+\pi^-)}{\sigma(B_c' + X)\mathcal{B}(B_c' \to B_c + \pi^+\pi^-)}. \quad (28)$$

At $\sqrt{s} = 13$ TeV, the ratio of cross sections is nearly 2.5. Taking account of the branching fractions, we estimate $\mathcal{R} \approx 2$. If B_c^* and B_c were produced with equal frequency, we would find $\mathcal{R} \approx 0.8$.

Now the CMS Collaboration [4] at the Large Hadron Collider, analyzing $140\,\text{fb}^{-1}$ of pp collisions at $\sqrt{s} = 13$ TeV, has observed a pattern that closely resembles the template of Fig. 7. In the distribution of $M(B_c\pi^+\pi^-) - M(B_c)^{\text{obs}} + M(B_c)$, they reconstruct a peak at 6871.0 ± 1.2 MeV,

which they identify as $B_c(2S)$, and a second peak 29.0 ± 1.5 MeV lower in mass (statistical errors only). (The observed B_c mass is replaced, event by event, with the world-average value to sharpen resolution.) The putative $B_c(2S)$ lies within 5 MeV of our expectation for the 2^1S_0 level, and the separation is to be compared with our expectation of 23 MeV. If we impose the scaling relation Eq. (13) for the hyperfine splittings, we reproduce the observed 29-MeV separation with $M(B_c^*) - M(B_c) = 68$ MeV, $M(B_c^{*'}) - M(B_c') = 39$ MeV. The $B_c^* \to B_c + \gamma$ photon momentum would be 68 MeV.

An unbinned extended maximum-likelihood fit to the CMS data returns 66 ± 10 events for the lower peak and 51 ± 10 for the upper. These yields are not yet corrected for detection efficiencies and acceptances, so they cannot be used to infer ratios of production cross sections times branching fractions. We look forward to the final result and to studies of the $\pi^+\pi^-$ invariant mass distribution as next steps in B_c spectroscopy.

Our calculations indicate that the $3S$ levels will lie above flavor threshold (see Sec. V C, especially the discussion surrounding Figs. 9 and 10), but it is conceivable that coupled-channel effects might push one or both states lower in mass. For that reason, it is worth examining the $B_c\pi^+\pi^-$ mass spectrum up through 7200 MeV for indications of $3^1S_0 \to B_c\pi^+\pi^-$ and $3^3S_1 \to B_c^*\pi^+\pi^-$ lines. According to our estimate of the $3S$ hyperfine splitting, the 3^3S_1 line would lie about 28 MeV below the 3^1S_0 line (36 MeV if we reset the $1S$ splitting to 68 MeV). For orientation, note that $\mathcal{B}(\Upsilon(3S) \to \Upsilon(1S)\pi^+\pi^-) = 4.37 \pm 0.08\%$, while 36% of $\Upsilon(3S)$ decays proceed through the ggg channel, which is not available to the $(c\bar{b})$ states. According to Table VIII, the $3S$ states are produced at approximately 44% of the rate for their $2S$ counterparts.

B. Electromagnetic transitions

It may in time become possible for experiments to detect some of the more energetic E1-transition photons that appear in Table VI. As an incentive for the search, we show in Fig. 8 the spectrum of E1 photons in decays of the 2^3S_1 and 2^1S_0 levels as well as the $2P \to 2S$ transitions, assuming as always a missing $B_c^* \to B_c\gamma$ photon in the reconstruction. Here we include direct production of the $2P$ states as well as feed-down from $2S \to 2P$ transitions. The strong $B_c^* \to B_c$ line arising from direct production of B_c^*, for which we calculate $\sigma \cdot \mathcal{B} \approx 225$ nb at $\sqrt{s} = 13$ TeV, is probably too low in energy to be observed. More promising are the $2P$ levels, which might show themselves in $B_c + \gamma$ invariant mass distributions. These lines make up the right-hand group (black lines) in Fig. 8. The $2^3P_2(6750) \to B_c^*\gamma$ line is a particularly attractive target for experiment because of the favorable production cross section, branching fraction, and 409-MeV photon energy. The $2P$ masses inferred from transitions to B_c^* will be shifted downward because of the unobserved M1 photon. It is not possible to produce
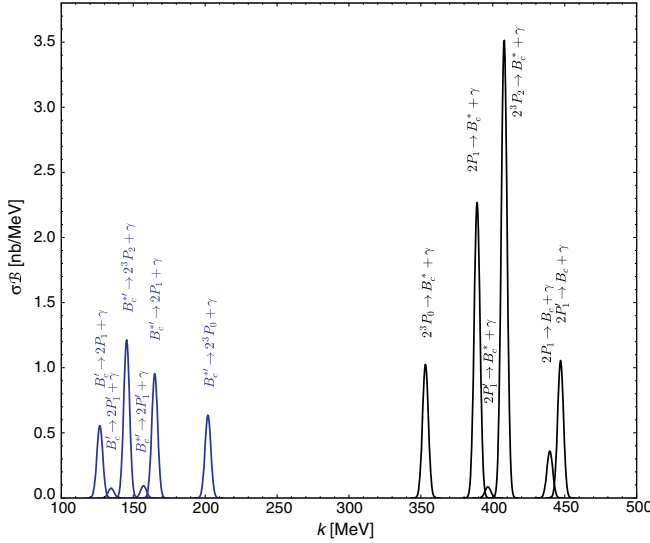
FIG. 8. Photon energies k and relative strengths of E1 transitions from $2S \to 2P$ (left group, blue curves) and $2P \to 1S$ (right group, black curves) $(c\bar{b})$ states. Production rates are taken from Table VIII and branching fractions from Table VI. We suppose that the photon transition $B_c^* \to B_c + \gamma$ goes unobserved in the cascade transitions. We assume Gaussian line shapes with standard deviation 2 MeV.

enriched samples of the $2S$ levels by tuning the energy of e^+e^- collisions, as is done for J/ψ and Υ, so reconstruction of the left-hand group of $2S \to 2P$ transitions (blue lines in Fig. 8) will be problematic.

In the far future, combining the photon transition energies and relative rates with expectations for production and decay may eventually make it possible to disentangle mixing of the spin-singlet and spin-triplet $J = L$ states.
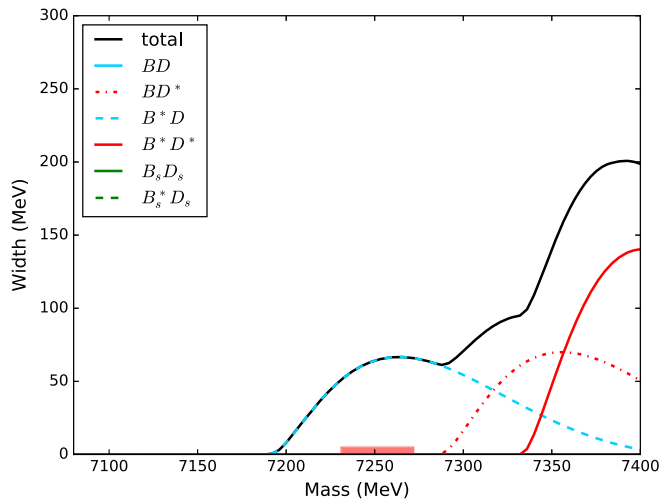
FIG. 9. Strong decay widths of the 3^1S_0 $(c\bar{b})$ level near open-flavor threshold. The shaded band on the mass axis indicates ± 20 MeV around our nominal value for the mass of this state, 7253 MeV.
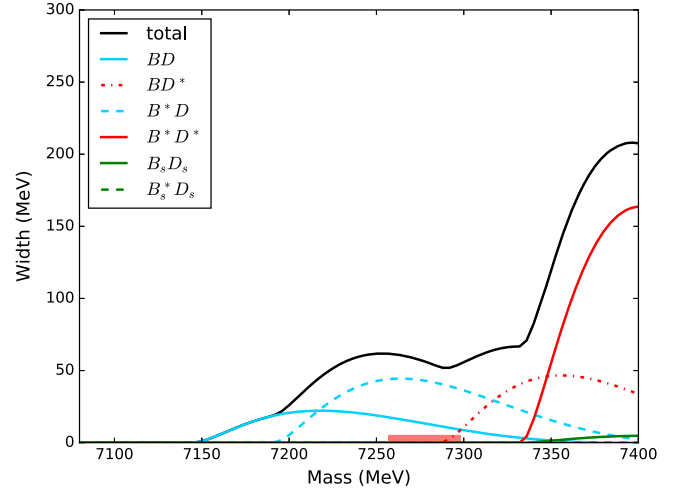

FIG. 10. Strong decay widths of the 3^3S_1 $(c\bar{b})$ level near open-flavor threshold. The shaded band on the mass axis indicates ± 20 MeV around our nominal value for the mass of this state, 7279 MeV.

C. States above open-flavor threshold

We estimate the strong decay rates for $(c\bar{b})$ states that lie above flavor threshold using the Cornell coupled-channel formalism [22] that we elaborated and applied to charmonium states in [23].

We expect both the 3^1S_0 and 3^3S_1 states to lie above threshold for strong decays. The 3^1S_0 state can decay into the final state B^*D and the 3^3S_1 level can decay into both the BD and B^*D final states. The open decay channels as a function of the masses of these states is shown in Figs. 9 and 10.
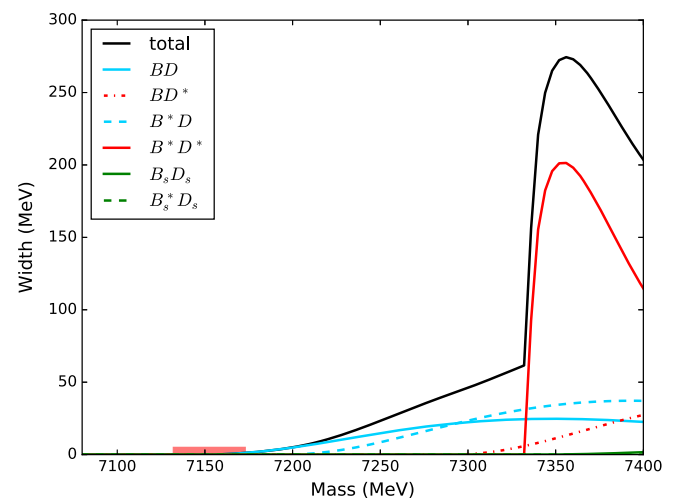

FIG. 11. Strong decay widths of the 3^3P_2 $(c\bar{b})$ level near open-flavor threshold. The shaded band on the mass axis indicates ± 20 MeV around our nominal value for the mass of this state, 7154 MeV.
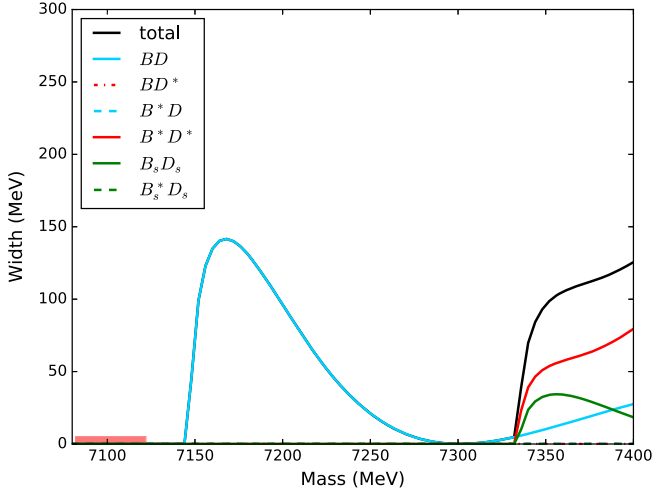
FIG. 12. Estimated strong decay widths of the 3^3P_0 ($c\bar{b}$) level near open-flavor threshold. The shaded band on the mass axis indicates ± 20 MeV around our nominal value for the mass of this state, 7104 MeV.

The 3^3P_2 state might be observed as a very narrow (d-wave) BD line near open-flavor threshold. Its decay width as a function of mass for the $2P$ states is given in Fig. 11.

In the phenomenological models the remaining $3P$ states lie just below the thresholds for strong decays. However, they are near enough to these thresholds that there might be interesting behavior at the threshold for B^*D in the $3P_1^{(\prime)}$ cases and for the BD threshold in the case of the 3^3P_0 state. Figure 12 shows that the 3^3P_0 width grows rapidly just above threshold. The strong decay widths as a function of mass for the $3P_1$ and $3P_1'$ states have a common behavior, displayed in Fig. 13.
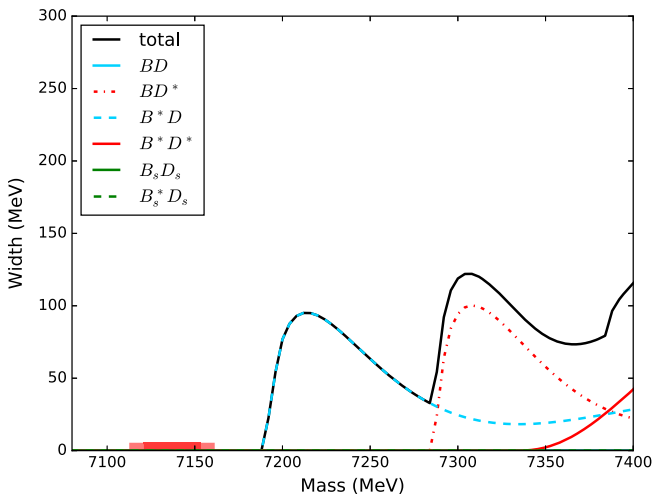

FIG. 13. Strong decay widths of the $3P_1$ or $3P_1^{(\prime)}$. The shaded band on the mass axis indicates ± 20 MeV around our nominal values for the masses of these state, 7135 and 7143 MeV.

It is worth keeping in mind that while narrow BD peaks may signal excited $(c\bar{b})$ levels, narrow $\bar{B}D$ peaks could indicate nearly bound $bc\bar{q}_k\bar{q}_l$ tetraquark states [47].

VI. TERA-Z PROSPECTS

In response to the discovery of the 125-GeV Higgs boson, $H(125)$ [48], plans for large circular electron-positron colliders (FCC-ee [49] and CEPC [50]) are being developed as $e^+e^- \to HZ^0$ "Higgs factories" to run at c.m. energy $\sqrt{s} \approx 240$ GeV. As now envisioned, these machines would have the added capability of high-luminosity running at $\sqrt{s} = M_Z$ that would accumulate 10^{12} examples of the reaction $e^+e^- \to Z^0$. With the observed branching fraction, $\mathcal{B}(Z^0 \to b\bar{b}) = (15.12 \pm 0.05)\%$ [12], the tera-Z mode would produce some 3×10^{11} boosted b-quarks, which would enable high-sensitivity searches for $(c\bar{b})$ states in a variety of decay channels. A recent computation suggests that $\mathcal{B}(Z^0 \to (c\bar{b}) + X) \approx 6 \times 10^{-4}$ [51].

The largest existing $e^+e^- \to Z^0 \to$ hadrons datasets were recorded by experiments at CERN's Large Electron-Positron Collider during the 1990s. In samples of (3.02, 3.9, and 4.2) million hadronic Z^0 decays, the DELPHI, ALEPH, and OPAL Collaborations [52] found a small number of candidates for the decays $B_c \to J/\psi\pi^+$, $J/\psi\ell^+\nu$ and $J/\psi 3\pi$. Those few specimens were not sufficient to establish a discovery, but the experiments were able to bound combinations of branching fractions $\mathcal{B}$ as

$$\frac{\mathcal{B}(Z^0 \to B_c + X)}{\mathcal{B}(Z^0 \to \text{hadrons})}\mathcal{B}\left(B_c \to \left\{ \begin{array}{c} J/\psi\pi^+ \\ J/\psi\ell^+\nu \\ J/\psi 3\pi \end{array} \right\} \right) \lesssim \text{few} \times 10^{-4},$$

(29)

at 90% confidence level, where X denotes anything. The relative simplicity of $e^+e^- \to Z^0$ events and the boosted kinematics of resulting B_c mesons suggest that a tera-Z factory might be a felicitous choice to investigate $2P \to 1S + \gamma$ lines.

VII. CONCLUSIONS AND OUTLOOK

In this article, we have presented a new analysis of the spectrum of mesons with beauty and charm. First, we modified the traditional Coulomb-plus-linear form of the quarkonium potential to incorporate running of the strong coupling constant α_s that saturates at a fixed value at long distances. The new frozen-α_s potential incorporates both perturbative and nonperturbative aspects of quantum chromodynamics. Second, we have set aside the perturbative treatment of spin splittings, instead incorporating lessons from lattice QCD and observations of the $(c\bar{c})$ and $(b\bar{b})$ spectra.

We look forward to additional experimental progress, first by confirming and elaborating the characteristics of the $2S$ levels reported by the CMS Collaboration [4]. Key observables are the mass of the 2^1S_0 state, the splitting between the two lines, and the ratio of peak heights corrected for efficiencies and acceptance. It is also of interest to test whether the dipion mass spectra in the cascade decays $B'_c \to B_c \pi^+ \pi^-$ and $B^{*\prime}_c \to B^*_c \pi^+ \pi^-$ follow the pattern seen in $\psi(2S) \to J/\psi \pi^+ \pi^-$ and $\Upsilon(2S) \to \Upsilon(1S) \pi^+ \pi^-$ decays. Although we expect the $3S$ levels to lie above flavor threshold, exploring the $B_c \pi^+ \pi^-$ mass spectrum up through 7200 MeV might yield indications of $3^1S_0 \to B_c \pi^+ \pi^-$ and $3^3S_1 \to B^*_c \pi^+ \pi^-$ lines. The presence of one or the other of these could signal interactions of bound states with open channels. Prospecting for narrow $B^{(*)}D^{(*)}$ peaks near threshold could yield evidence of B_c states beyond the $2S$ levels.

The next frontier is the search for radiative transitions among $(c\bar{b})$ levels. The most promising candidate for first light is the $2^3P_2(6750) \to B^*_c \gamma$ transition. Determining the B^*_c mass, perhaps by reconstructing $B^*_c \to B_c \gamma$, would provide an important check on lattice QCD calculations and a key input to future calculations.

Detecting the $B_c \to \tau \nu_\tau$ and $B_c \to p\bar{p}\pi^+$ decays would be impressive experimental feats and would provide another test of the short-distance behavior of the ground-state wave function, complementing what will be learned from the B^*_c–B_c splitting.

ACKNOWLEDGMENTS

APPENDIX: STRONG COUPLING EVOLUTION

To make calculations with the frozen-α_s potential, one must combine a linear term with a Coulomb term, $-4\alpha_s(r)/3r$, for which $\alpha_s(r)$ is characterized by the solid red curve of Fig. 1. We present in Table IX numerical values of the strong coupling over the relevant range of distances, $0 \le r \le 0.8$ fm. The entries advance in steps of $\delta \ln r = 0.1$.

TABLE IX. Evolution of the strong coupling.

r (fm)	$\alpha_s(r)$
0.0080	0.1706
0.0088	0.1742
0.0097	0.1780
0.0108	0.1819
0.0119	0.1862
0.0132	0.1908
0.0145	0.1957
0.0161	0.2007
0.0178	0.2061
0.0196	0.2116
0.0217	0.2174
0.0240	0.2235
0.0265	0.2299
0.0293	0.2365
0.0323	0.2434
0.0358	0.2505
0.0395	0.2579
0.0437	0.2659
0.0483	0.2743
0.0533	0.2829
0.0589	0.2915
0.0651	0.3001
0.0720	0.3087
0.0796	0.3171
0.0879	0.3252
0.0972	0.3330
0.1074	0.3403
0.1187	0.3471
0.1312	0.3533
0.1450	0.3590
0.1602	0.3640
0.1771	0.3685
0.1957	0.3723
0.2163	0.3757
0.2390	0.3786
0.2642	0.3811
0.2920	0.3832
0.3227	0.3849
0.3566	0.3864
0.3941	0.3876
0.4355	0.3886
0.4813	0.3895
0.5320	0.3902
0.5879	0.3908
0.6497	0.3913
0.7181	0.3917
0.7936	0.3920

[1] G. Aad *et al.* (ATLAS Collaboration), Observation of an Excited $B_c^\pm$ Meson State with the ATLAS Detector, Phys. Rev. Lett. **113,** 212004 (2014).

[2] R. Aaij *et al.* (LHCb Collaboration), Search for excited B_c^+ states, J. High Energy Phys. 01 (2018) 138.

[3] For a recent assessment, see contributions to the Micro Workshop on B_c^+ physics at LHCb, 13 July 2016, https://indico.cern.ch/event/549155/, especially Z. Yang, Experiment—Recent history of the B_c^+ meson, https://indico.cern.ch/event/549155/contributions/2226387/attachments/1308369/1957602/Bc_results20160713.pdf; A. Luchinsky, Theory–Status of the theoretical description of the B_c^+ meson, https://indico.cern.ch/event/549155/contributions/2226440/attachments/1308367/1956579/bc_Luchinsky.pdf; R. Oldeman, Experiment—Perspectives for future studies, https://indico.cern.ch/event/549155/contributions/2226443/attachments/1308858/1957460/20160713_Bc.pdf; A. V. Berezhnoy, Theory–B_c^+ production and spectroscopy, https://indico.cern.ch/event/549155/contributions/2226438/attachments/1309000/1957694/Berezhnoy_Bc.pdf.

[4] A. M. Sirunyan *et al.* (CMS Collaboration), Observation of two excited B_c^+ states and measurement of the B_c^+ (2S) mass in pp collisions at $\sqrt{s} = 13$ TeV, arXiv:1902.00571.

[5] E. Eichten and F. Feinberg, Spin dependent forces in QCD, Phys. Rev. D **23,** 2724 (1981).

[6] E. J. Eichten and C. Quigg, Mesons with beauty and charm: Spectroscopy, Phys. Rev. D **49,** 5845 (1994).

[7] For other work in a similar spirit, see V. V. Kiselev, A. K. Likhoded, and A. V. Tkabladze, B_c spectroscopy, Phys. Rev. D **51,** 3613 (1995); L. P. Fulcher, Phenomenological predictions of the properties of the B_c system, Phys. Rev. D **60,** 074006 (1999); S. Godfrey and N. Isgur, Mesons in a relativized quark model with chromodynamics, Phys. Rev. D **32,** 189 (1985); S. Godfrey, Spectroscopy of B_c mesons in the relativized quark model, Phys. Rev. D **70,** 054017 (2004); D. Ebert, R. N. Faustov, and V. O. Galkin, Properties of heavy quarkonia and B_c mesons in the relativistic quark model, Phys. Rev. D **67,** 014027 (2003); A. V. Berezhnoy, V. V. Kiselev, A. K. Likhoded, and A. I. Onishchenko, B_c meson at LHC, Yad. Fiz. **60N10,** 1889 (1997) [Phys. At. Nucl. **60,** 1729 (1997)]; N. R. Soni, B. R. Joshi, R. P. Shah, H. R. Chauhan, and J. N. Pandya, $Q\bar{Q}$ ($Q \in \{b, c\}$) spectroscopy using the Cornell potential, Eur. Phys. J. C **78,** 592 (2018).

[8] F. Abe *et al.* (CDF Collaboration), Observation of the B_c Meson in $p\bar{p}$ Collisions at $\sqrt{s} = 1.8$ TeV, Phys. Rev. Lett. **81,** 2432 (1998).

[9] T. Aaltonen *et al.* (CDF Collaboration), Observation of the Decay $B_c^+ \to J/\psi\pi^\pm$ and Measurement of the B_c^+ Mass, Phys. Rev. Lett. **100,** 182002 (2008).

[10] V. M. Abazov *et al.* (D0 Collaboration), Observation of the B_c Meson in the Exclusive Decay $B_c \to J/\psi\pi$, Phys. Rev. Lett. **101,** 012001 (2008).

[11] R. Aaij *et al.* (LHCb Collaboration), Measurements of B_c^+ Production and Mass with the $B_c^+ \to J/\psi\pi^+$ Decay, Phys. Rev. Lett. **109,** 232001 (2012); Observation of $B_c^+ \to J/\psi D_s^+$ and $B_c^+ \to J/\psi D_s^{*+}$ decays, Phys. Rev. D **87,** 112012 (2013); Publisher's Note **89,** 019901(A) (2014);

First Observation of a Baryonic B_c^+ Decay, Phys. Rev. Lett. **113,** 152003 (2014).

[12] M. Tanabashi *et al.* (Particle Data Group), Review of particle physics, Phys. Rev. D **98,** 030001 (2018).

[13] I. F. Allison, C. T. H. Davies, A. Gray, A. S. Kronfeld, P. B. Mackenzie, and J. N. Simone (Fermilab Lattice, HPQCD, and UKQCD Collaborations), Mass of the B_c Meson in Three-Flavor Lattice QCD, Phys. Rev. Lett. **94,** 172001 (2005).

[14] R. J. Dowdall, C. T. H. Davies, T. C. Hammant, and R. R. Horgan, Precise heavy-light meson masses and hyperfine splittings from lattice QCD including charm quarks in the sea, Phys. Rev. D **86,** 094510 (2012).

[15] We use spectroscopic notation $n^{2S+1}L_J$, where n is the principal quantum number, S is total spin, and $L = S, P, D, \dots$ represents the angular momentum $0, 1, 2, \dots$.

[16] M. Beneke and G. Buchalla, The B_c meson lifetime, Phys. Rev. D **53,** 4991 (1996); A. Yu. Anisimov, I. M. Narodetsky, C. Semay, and B. Silvestre-Brac, The B_c meson lifetime in the light front constituent quark model, Phys. Lett. B **452,** 129 (1999); V. V. Kiselev, A. E. Kovalsky, and A. K. Likhoded, B_c decays and lifetime in QCD sum rules, Nucl. Phys. **B585,** 353 (2000); C.-H. Chang, S.-L. Chen, T.-F. Feng, and X.-Q. Li, The lifetime of B_c meson and some relevant problems, Phys. Rev. D **64,** 014003 (2001).

[17] N. Brambilla *et al.* (Quarkonium Working Group), Heavy quarkonium physics, CERN Yellow Report No. CERN-2005-005, 2005, DOI: 10.5170/CERN-2005-005.

[18] A. Ali, L. Maiani, A. D. Polosa, and V. Riquer, $B_c^\pm$ decays into tetraquarks, Phys. Rev. D **94,** 034036 (2016); A. Esposito, M. Papinutto, A. Pilloni, A. D. Polosa, and N. Tantalo, Doubly charmed tetraquarks in B_c and Ξ_{bc} decays, Phys. Rev. D **88,** 054029 (2013); W. Wang, Y.-L. Shen, and C.-D. Lu, The study of $B_c^- \to X(3872)\pi^-(K^-)$ decays in the covariant light-front approach, Eur. Phys. J. C **51,** 841 (2007); W. Wang and Q. Zhao, Decipher the short-distance component of $X(3872)$ in B_c decays, Phys. Lett. B **755,** 261 (2016).

[19] A. Lytle, B. Colquhoun, C. Davies, and J. Koponen, B_c spectroscopy using highly improved staggered quarks, Proc. Sci. LATTICE2018 (**2018**) 083.

[20] T. Appelquist and H. D. Politzer, Heavy Quarks and e^+e^- Annihilation, Phys. Rev. Lett. **34,** 43 (1975).

[21] T. Appelquist, A. De Rujula, H. D. Politzer, and S. L. Glashow, Spectroscopy of the New Mesons, Phys. Rev. Lett. **34,** 365 (1975); E. Eichten, K. Gottfried, T. Kinoshita, J. B. Kogut, K. D. Lane, and T.-M. Yan, Spectrum of Charmed Quark-Antiquark Bound States, Phys. Rev. Lett. **34,** 369 (1975); Erratum, Phys. Rev. Lett. **36,** 1276(E) (1976).

[22] E. Eichten, K. Gottfried, T. Kinoshita, K. D. Lane, and T.-M. Yan, Charmonium: The Model, Phys. Rev. D **17,** 3090 (1978); , Charmonium: The Model, Phys. Rev. D **21,** 313(E) (1980); Charmonium: Comparison with experiment, Phys. Rev. D **21,** 203 (1980).

[23] E. J. Eichten, K. Lane, and C. Quigg, Charmonium levels near threshold and the narrow state $X(3872) \to \pi^+\pi^-J/\psi$, Phys. Rev. D **69,** 094019 (2004); New states above charm threshold, Phys. Rev. D **73,** 014014 (2006); Erratum, Phys. Rev. D **73,** 079903(E) (2006).

[24] N. Brambilla *et al.*, Heavy quarkonium: Progress, puzzles, and opportunities, Eur. Phys. J. C **71**, 1534 (2011).

[25] Y. Sumino, Computation of heavy quarkonium spectrum in perturbative QCD, Proc. Sci. LL2016 (**2016**) 011.

[26] A. Martin, A fit of upsilon and charmonium spectra, Phys. Lett. **93B**, 338 (1980).

[27] J. L. Richardson, The heavy quark potential and the Υ, J/ψ systems, Phys. Lett. **82B**, 272 (1979).

[28] W. Buchmüller and S. H. H. Tye, Quarkonia and quantum chromodynamics, Phys. Rev. D **24**, 132 (1981).

[29] V. N. Gribov, The theory of quark confinement, Eur. Phys. J. C **10**, 91 (1999).

[30] K. G. Chetyrkin, Four-loop renormalization of QCD: Full set of renormalization constants and anomalous dimensions, Nucl. Phys. **B710**, 499 (2005); M. Czakon, The Four-loop QCD beta-function and anomalous dimensions, Nucl. Phys. **B710**, 485 (2005).

[31] M. Jeżabek, M. Peter, and Y. Sumino, On the relation between QCD potentials in momentum and position space, Phys. Lett. B **428**, 352 (1998).

[32] D. Gromes, Spin dependent potentials in QCD and the correct long range spin orbit term, Z. Phys. C **26**, 401 (1984).

[33] C. T. H. Davies, K. Hornbostel, G. P. Lepage, A. J. Lidsey, J. Shigemitsu, and J. H. Sloan, B_c spectroscopy from lattice QCD, Phys. Lett. B **382**, 131 (1996).

[34] E. B. Gregory, C. T. H. Davies, E. Follana, E. Gamiz, I. D. Kendall, G. P. Lepage, H. Na, J. Shigemitsu, and K. Y. Wong, A Prediction of the B_c^* Mass in Full Lattice QCD, Phys. Rev. Lett. **104**, 022001 (2010).

[35] N. Mathur, M. Padmanath, and S. Mondal, Precise Predictions of Charmed-Bottom Hadrons from Lattice QCD, Phys. Rev. Lett. **121**, 202002 (2018).

[36] C. Quigg and J. L. Rosner, Counting narrow levels of quarkonium, Phys. Lett. **72B**, 462 (1978).

[37] E. Eichten and K. Gottfried, Heavy quarks in e^+e^- annihilation, Phys. Lett. **66B**, 286 (1977).

[38] L. S. Brown and R. N. Cahn, Chiral Symmetry and $\psi' \rightarrow \psi\pi\pi$ Decay, Phys. Rev. Lett. **35**, 1 (1975).

[39] See Sec. 7 of Ref. [17] and Sec. 3.3 of Ref. [24] for surveys of cascade decays.

[40] We adopt the conventional normalization, $\int d\Omega$: $Y^*_{\ell m}(\theta, \phi)Y_{\ell' m'}(\theta, \phi) = \delta_{\ell\ell'}\delta_{mm'}$. See, e.g., the Appendix of H. A. Bethe and E. E. Salpeter, *Quantum Mechanics of One- and Two-Electron Atoms* (Springer-Verlag, Berlin, 1957).

[41] R. Van Royen and V. F. Weisskopf, Hadron decay processes and the quark model, Nuovo Cimento A **50**, 617 (1967); Erratum, Nuovo Cimento A **51**, 583(E) (1967). The factor of 3 accounts for quark color.

[42] E. Braaten and S. Fleming, QCD radiative corrections to the leptonic decay rate of the B_c meson, Phys. Rev. D **52**, 181 (1995); A. V. Berezhnoy, V. V. Kiselev, and A. K. Likhoded,

Photonic production of S- and P wave B_c states and doubly heavy baryons, Z. Phys. A **356**, 89 (1996).

[43] B. Colquhoun, C. T. H. Davies, R. J. Dowdall, J. Kettle, J. Koponen, G. P. Lepage, and A. T. Lytle (HPQCD Collaboration), B-meson decay constants: A more complete picture from full lattice QCD, Phys. Rev. D **91**, 114509 (2015); For further work on semileptonic decays, see A. Lytle, B. Colquhoun, C. Davies, J. Koponen, and C. McNeile, Semileptonic B_c decays from full lattice QCD, Proc. Sci., BEAUTY2016 (**2016**) 069; A. Lytle, Theory—Semileptonic B_c^+ decays and Lattice QCD, in Ref. [3], https://indico.cern.ch/event/549155/contributions/2226442/attachments/1308725/1957203/Bc_lattice.pdf.

[44] M. J. Baker, J. Bordes, C. A. Dominguez, J. Penarrocha, and K. Schilcher, B meson decay constants f_{B_c}, f_{B_s} and f_B from QCD sum rules, J. High Energy Phys. 07 (2014) 032.

[45] C.-H. Chang, J.-X. Wang, and X.-G. Wu, BCVEGPY2.0: An upgraded version of the generator BCVEGPY with the addition of hadroproduction of the P-wave B_c states, Comput. Phys. Commun. **174**, 241 (2006). We use (derivatives of) wave functions at the origin derived from our current work. The quark mass parameters in this program vary with the produced state, to reproduce its mass. $1S: m_b = 5.000$, $m_c = 1.275$; $2S: m_b = 5.234$, $m_c = 1.633$; $2P: m_b = 5.184$, $m_c = 1.573$; $3S: m_b = 5.447$, $m_c = 1.825$; $3P: m_b = 5.502$, $m_c = 1.633$, all in GeV.

[46] In an effective power-law potential $V(r) = \lambda r^\nu$, $\Delta_{21} < 0$ so long as $\nu < 1$. See Secs. 4.1.1 and 5.3.2 of C. Quigg and J. L. Rosner, Quantum mechanics with applications to quarkonium, Phys. Rep. **56**, 167 (1979), particularly Eqs. (4.21) and (4.22).

[47] E. J. Eichten and C. Quigg, Heavy-Quark Symmetry Implies Stable Heavy Tetraquark Mesons $Q_iQ_j\bar{q}_k\bar{q}_l$, Phys. Rev. Lett. **119**, 202002 (2017).

[48] G. Aad *et al.* (ATLAS Collaboration), Observation of a new particle in the search for the Standard Model Higgs boson with the ATLAS detector at the LHC, Phys. Lett. B **716**, 1 (2012); S. Chatrchyan *et al.* (CMS Collaboration), Observation of a new boson at a mass of 125 GeV with the CMS experiment at the LHC, Phys. Lett. B **716**, 30 (2012).

[49] FCC-ee, the electron-positron option of the future circular colliders design study, http://tlep.web.cern.ch.

[50] CEPC, Circular electron-positron collider, http://cepc.ihep.ac.cn.

[51] Q.-L. Liao, Y. Yu, Y. Deng, G.-Y. Xie, and G.-C. Wang, Excited heavy quarkonium production via Z^0 decays at a high luminosity collider, Phys. Rev. D **91**, 114030 (2015).

[52] P. Abreu *et al.* (DELPHI Collaboration), Search for the B_c meson, Phys. Lett. B **398**, 207 (1997); R. Barate *et al.* (ALEPH Collaboration), Search for the B_c meson in hadronic Z decays, Phys. Lett. B **402**, 213 (1997); K. Ackerstaff *et al.* (OPAL Collaboration), Search for the B_c meson in hadronic Z^0 decays, Phys. Lett. B **420**, 157 (1998).